Phys Chem Minerals
DOI 10.1007/s00269-006-0105-y

ORIGINAL PAPER

Pressure effect on the electronic structure of iron in $(Mg,Fe)(Si,Al)O_3$ perovskite: a combined synchrotron Mössbauer and X-ray emission spectroscopy study up to 100 GPa

J. Li · W. Sturhahn · J. M. Jackson · V. V. Struzhkin · J. F. Lin · J. Zhao · H. K. Mao · G. Shen

Received: 21 February 2006 / Accepted: 24 July 2006

Abstract We investigated the valence state and spin state of iron in an Al-bearing ferromagnesian silicate perovskite sample with the composition $(Mg_{0.88}Fe_{0.09})(Si_{0.94}Al_{0.10})O_3$ between 1 bar and 100 GPa and at 300 K, using diamond cells and synchrotron Mössbauer spectroscopy techniques. At pressures below 12 GPa, our Mössbauer spectra can be sufficiently fitted by a ''two-doublet'' model, which assumes one ferrous Fe^{2+}-like site and one ferric Fe^{3+}-like site with distinct hyperfine parameters. The simplest interpretation that is consistent with both the Mössbauer data and previous X-ray emission data on the same sample is that the Fe^{2+}-like site is high-spin Fe^{2+}, and the Fe^{3+}-like site is high-spin Fe^{3+}. At 12 GPa and higher pressures, a ''three-doublet'' model is necessary and sufficient to fit the Mössbauer spectra. This model assumes two Fe^{2+}-like sites and one Fe^{3+}-like site distinguished by their hyperfine parameters. Between 12 and 20 GPa, the fraction of the Fe^{3+}-like site, $Fe^{3+}/\sum Fe$, changes abruptly from about 50 to 70%, possibly due to a spin crossover in six-coordinate Fe^{2+}. At pressures above 20 GPa, the fractions of all three sites remain unchanged to the highest pressure, indicating a fixed valence state of iron within this pressure range. From 20 to 100 GPa, the isomer shift between the Fe^{3+}-like and Fe^{2+}-like sites increases slightly, while the values and widths of the quadruple splitting of all three sites remain essentially constant. In conjunction with the previous X-ray emission data, the Mössbauer data suggest that Fe^{2+} alone, or concurrently with Fe^{3+}, undergoes pressure-induced spin crossover between 20 and 100 GPa.

Keywords Aluminum-bearing perovskite · Valence state · Spin crossover · Synchrotron Mössbauer spectroscopy · X-ray emission spectroscopy · Pressure effect

J. Li (✉) · J. M. Jackson
Department of Geology, University of Illinois at Urbana Champaign, 245 Natural History Building, 1301 West Green Street, Urbana, IL 61801, USA
e-mail: jackieli@uiuc.edu

W. Sturhahn · J. Zhao · H. K. Mao · G. Shen
Advanced Photon Source, Argonne National Laboratory, Argonne, IL 60439, USA

V. V. Struzhkin · J. F. Lin · J. M. Jackson · H. K. Mao · G. Shen
Geophysical Laboratory, Carnegie Institution of Washington, Washington, DC 20015, USA

J. F. Lin
Lawrence Livermore National Laboratory, Livermore, CA 94550, USA

Introduction

Aluminum-bearing ferromagnesian silicate perovskite (hereafter referred to as ''Al-PV'') is believed to be the most abundant phase in the Earth's interior (e.g. Anderson and Bass 1986; Liu 1974). It represents at least one third of the total mass of our planet, more than any other terrestrial phase. Theoretical considerations and experimental investigations showed that the valence state and spin state of iron can significantly affect the crystal chemistry, density, thermal conductivity and electrical conductivity of its host phases (Burns 1993; Badro et al. 2003; 2004; Fei et al. 2005; Lin et al. 2005; Shannon and Prewitt 1969; Speziale

et al. 2005; Wood and Rubie 1996; Xu et al. 1998). Given its potentially far-reaching consequences, accurate characterization of the electronic structure of iron in Al-PV under the lower mantle pressure conditions is necessary for our understanding of the nature and dynamics of the Earth's deep interior.

A number of studies have been carried out to investigate the electronic structure of iron in Al-PV, including ^{57}Fe conventional Mössbauer spectroscopy and electron energy loss spectroscopy (EELS) at ambient conditions (Lauterbach et al. 2000; McCammon 1997; McCammon et al. 2004; Frost et al. 2004), X-ray emission spectroscopy (XES) up to Mbar pressure at ambient temperature (Li et al. 2004), and first-principle computations (Li et al. 2005). There are also numerous investigations on the electronic structure of iron in Al-free PV (Jackson et al. 2005 and references therein). The Mössbauer and EELS data suggest that the fraction of ferric ion (Fe^{3+}) in Al-PV is a function of the Al content (Lauterbach et al. 2000; McCammon 1997; McCammon et al. 2004; Frost et al. 2004). The XES study revealed a pressure-induced gradual loss of magnetic moment in one Al-PV sample between 20 and 100 GPa, indicating possible occurrence of mixed-spin state and intermediate-spin state under high pressures (Li et al. 2004). The first-principle computation results show that Fe^{3+} undergoes a high-spin to low-spin crossover between 97 and 126 GPa and at 300 K, with no stability field for the intermediate-spin state (Li et al. 2005).

To date in situ measurements on the valence state of iron in Al-PV have not been performed under high pressures. Mössbauer spectroscopy is an established method for investigating the valence state of iron (e.g. Bancroft et al. 1967; Wertheim 1964). Recent developments in synchrotron Mössbauer spectroscopy (SMS) have enabled in situ measurements of small samples (<10 μm in thickness) with relatively low iron contents (<10 at%) to Mbar pressures (Jackson et al. 2005). The combination of electronic spectroscopy with Mössbauer spectroscopy played crucial roles in detecting the pressure-induced spin transition in FeS at 6.7 GPa and 300 K (King et al 1978; Rueff et al. 1999), and in identifying the intermediate-spin state in iron-bearing compounds (Bancroft 1973). In this study, we apply the SMS techniques to the same Al-PV sample that was studied previously using the XES techniques (Li et al. 2004), in order to monitor the valence state of iron as a function of pressure, and to derive new constraints on the spin state evolution of iron in Al-PV under lower mantle pressures.

Experimental method

Synchrotron Mössbauer spectroscopy experiments

Immediately following the X-ray emission study (Li et al. 2004), SMS measurements were carried out at beamline 3-ID of the Advanced Photon Source, Argonne National Laboratory. Three fragments of samples were investigated: One fragment was glued to a beryllium foil for measurements at ambient conditions, a second fragment was loaded into a wide-angle panoramic cell (Mao et al. 2001), and the third fragment was loaded into a separate diamond anvil cell that was first used for the XES study to 100 GPa (Li et al. 2004), and then used for SMS measurements at 100 and 80 GPa. In the panoramic cell, two flat diamonds with 600 μm culet size were mounted on carbide seats. An X-ray transparent beryllium disc (1 mm thick, 5 mm in diameter) was pre-indented to 50 μm thickness and drilled to create a 300 μm gasket hole. The hole was filled with amorphous boron, which was pressed between the two diamonds. A 100 μm hole was drilled into the compressed boron to create a sample chamber, in which a fragment of Al-PV and several ruby grains were loaded. The use of boron inner gasket with high shear strength helps to maximize the thickness of the sample chamber under pressure and increases the pressure homogeneity (Lin et al. 2003). In the cell from the XES study, high pressure was generated using a symmetrical piston-cylinder type diamond-anvil cell (Mao et al. 2001). Two beveled diamonds (about 300 μm bevel size and 150 μm flat culet size) were mounted in the cell. An X-ray transparent beryllium disc (1 mm thick and 5 mm in diameter) was pre-indented to about 20 μm in thickness then drilled to create a 50-μm-sized sample chamber. A piece of Al-PV sample and a few grains of ruby were loaded into the chamber and sandwiched between the two diamonds. Sample pressure was determined from the laser-induced fluorescence spectrum of ruby (Mao et al. 1986; Zha et al. 2000). Near 100 GPa, the ruby pressures were confirmed by the positions of the Raman peaks of the diamonds.

The details of the SMS measurements are similar to that described in Jackson et al. (2005). The electron storage ring was operated in top-up mode with 23 bunches that were separated by 153 ns. The incident X-ray with a bandwidth of 1 meV was tuned to the nuclear transition energy of ^{57}Fe (14.4125 keV) using multiple-crystal Bragg reflection monochromators (Toellner 2000). It was then focused to a spot size of 6×6 μm^2 at the full-width half-maximum (FWHM) using a Kirkpatrik-Baez mirror system (Eng et al. 1998). With a

flux of 10^9 photons/s at the focal spot, sufficient counting rate could be obtained on the small sample over half an hour of acquisition time period. Nuclear resonant scattering was observed in a time window of 20–120 ns following excitation. Time spectra were collected at ambient conditions on the Al-PV fragment loaded onto a piece of beryllium foil, at 2–30 GPa on the Al-PV fragment loaded in the panoramic cell, and at 100 and 80 GPa on the Al-PV fragment in the symmetrical piston-cylinder type cell from the XES study.

Evaluation of time spectra

The synchrotron Mössbauer spectroscopic data were evaluated following the same procedure as described in Jackson et al. (2005). The CONUSS software was used for analysis (Sturhahn 2000; Sturhahn and Gerdau 1994). For the fragment measured under ambient conditions the thickness was fixed at about 3 μm ^{57}Fe, equivalent to about 150 μm Al-PV. For the fragments in the diamond cells, we obtained 0.5 and 0.3 μm ^{57}Fe, equivalent to about 25 and 15 μm Al-PV, respectively. The results were found insensitive to the exact thickness values. Not always was it possible to vary all parameters simultaneously. This situation is indicated by values without errors (Table 1). The valence state of iron is associated with specific ranges of the hyperfine parameters derived from the synchrotron Mössbauer data. The distinctly different electric field gradients (EFGs) of Fe^{2+}- and Fe^{3+}-like crystal sites permit us to determine the $Fe^{3+}/\Sigma Fe$ ratio. At low pressures, a second Fe^{2+}-like site is not required, as indicated by the dashes in Table 1. The distribution functions of the quadrupole splittings are of Gaussian type, and widths are given at half the maximum of the Gaussian. The isomer shift for pressures below 100 GPa is given with respect to the Fe^{2+}, as no external standard reference absorber was used. With the exception of the 100 GPa data, a non-zero isomer shift between the two Fe^{2+}-like sites did not improve the fit quality. The isomer shift between the two Fe^{2+}-like sites was set to zero. At 100 GPa, the isomer shift between the Fe^{2+}-like sites is 0.10(1) mm/s.

Results and discussion

The measured time spectra are shown in Fig. 1 along with calculated curves using the best-fit parameters listed in Table 1. The weight fractions and hyperfine parameters of modeled iron sites as functions of pressure are plotted in Fig. 2. At 1 bar and 3 GPa, a ''two-doublet model'' provides a satisfactory fit to the spectrum. Under higher pressures, a ''three-doublet model'' containing two Fe^{2+}-like sites and one Fe^{3+}-like site is necessary and sufficient to fit the spectra. The two Fe^{2+}-like sites have the same isomer shift but distinct quadrupole splittings. We labeled the Fe^{2+}-like site with the smaller quadrupole splittings as $Fe^{2+}{}_1$. This site was present at ambient pressure. The Fe^{2+}-like site with the larger quadrupole splittings appeared upon compression and was denoted as $Fe^{2+}{}_2$. These doublets are broadened, probably due to distributed EFGs acting on the ^{57}Fe nuclei. The ''three-doublet model'' has been applied earlier to explain Mössbauer data on $(Fe,Mg)SiO_3$ perovskites at ambient pressure conditions (Fei et al. 1994) and in the high-pressure regime (Jackson et al. 2005).

Table 1 The best-fit parameters from Mössbauer spectroscopy measurements

P (GPa)	$Fe^{2+}{}_1$ fraction	QS (mm/s)	FWHM (mm/s)	$Fe^{2+}{}_2$ fraction	QS (mm/s)	FWHM (mm/s)	Fe^{3+} fraction	QS (mm/s)	FWHM (mm/s)	IS (mm/s)
SMS fragment 1										
0	–	–	–	0.46 (1)	2.11(1)	0.70 (1)	0.54	0.77(1)	0.31 (1)	–0.70 (1)
SMS fragment 2, wide-angle DAC										
3	–	–	–	0.47 (1)	2.09 (1)	1.19 (1)	0.53	0.90 (1)	0.48 (1)	–0.42 (1)
12	0.07 (1)	2.40 (1)	1.05	0.40 (1)	2.20 (1)	1.29 (1)	0.53	0.89 (1)	0.60 (1)	–0.32 (1)
20	0.09 (1)	3.49 (1)	0.35	0.13 (1)	2.65 (1)	0.26	0.78	0.89 (1)	0.83 (1)	–0.20 (1)
30	0.10 (1)	3.55 (1)	0.36	0.15 (1)	2.75 (1)	0.27 (1)	0.75	0.88 (1)	0.81 (1)	–0.21 (1)
SMS fragment 3, DAC ''009''										
80[a]	0.11 (1)	3.47 (1)	0.04	0.15 (1)	2.55 (4)	0.14 (5)	0.74	0.81 (2)	0.74 (9)	–0.14 (3)
100	0.11 (1)	3.45 (1)	0.03	0.15 (1)	2.60 (1)	0.08	0.74	0.80 (2)	0.75 (3)	–0.06 (1)

Conventional Mössbauer measurements found that $IS(Fe^{3+}) = 0.43$, $IS(Fe^{2+}) = 1.12$, with respect to alpha iron. Numbers in parenthesis are the uncertainties on the last reported digit, based on the 2σ of the fitted parameters

QS quadruple splitting, *FWHM* full width at half maximum of the QS, *IS* isomer shift between Fe^{3+} and Fe^{2+}

[a] Measured upon decompression

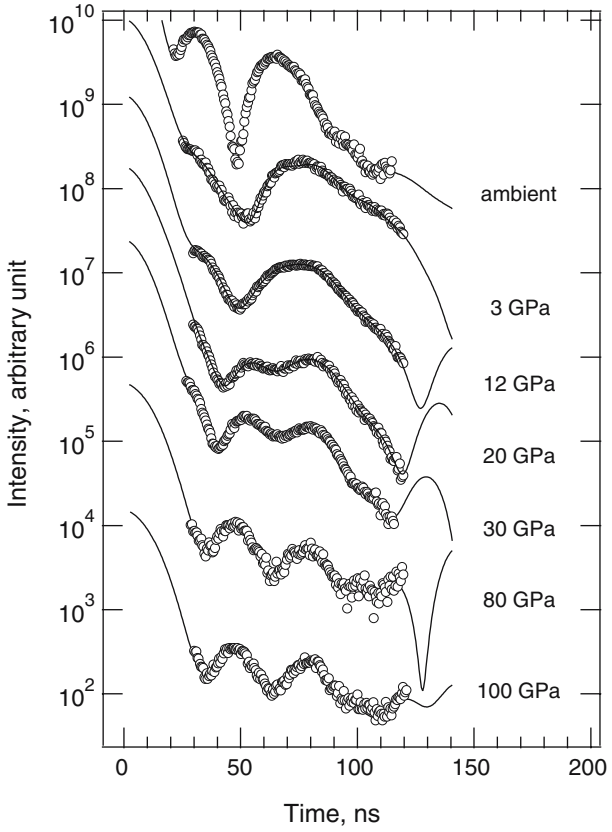

Fig. 1 SMS time spectra (*open circles*) and calculated curves with best-fit parameters given in Table 1 (*solid lines*). The spectra are vertically offset for clarity

Characteristic hyperfine parameters of iron

In Mössbauer spectroscopy, the hyperfine parameters of iron are determined by its valence state, spin state, and crystallographic site (Bancroft et al. 1967; Ingalls 1964; Wertheim 1964). The isomer shift and quadrupole splitting arise from the electrostatic interaction of a nucleus with its surrounding electronic charge. The isomer shift measures the shift of the nuclear levels due to a change in the *s*-electron density (Wertheim 1964). The configurations of valence electrons in iron metal, Fe^{2+}, and Fe^{3+} are $[Ar]3d^64s^2$, $[Ar]3d^6$, and $[Ar]3d^5$, respectively. Due to the screening effect of 3*d* electrons, the *s*-electron density at the nucleus is the highest in iron metal, and the lowest in Fe^{2+}, resulting in positive isomer shifts for Fe^{2+} (0.8–1.3 mm/s for six- or eight-coordinate sites in oxides) and Fe^{3+} (0.3–0.5 mm/s for six-coordinate sites in oxides) relative to iron metal (Bancroft et al. 1967). Experimental data on a number of sulfides show that a high-spin to low-spin transition in Fe^{2+} leads to a reduction in the isomer shift, consistent with an increase in the *s*-electron density as a result of volume contraction (King et al. 1978; Rueff et al. 1999). The isomer shift of low-spin Fe^{2+} is comparable to that of high-spin Fe^{3+}. Reduction of isomer shift is also observed on Fe^{3+} in several chemical compounds (Bancroft 1973). Limited data suggest that the isomer shifts of ferrous and ferric ions in the intermediate-spin state are indistinguishable from those in the low-spin state (Bancroft 1973). In this study, we measured the isomer shift between the Fe^{3+}-like site and Fe^{2+}-like sites. To facilitate data analysis, the ranges of literature values of isomer shift between high-spin Fe^{3+} and high-spin Fe^{2+} and that between high-spin Fe^{3+} and low-spin Fe^{2+} at ambient conditions are plotted in Fig. 2c as references.

Quadruple splitting is the result of the interaction between the nuclear quadrupole moment and the EFG. The two fundamental sources of the EFG are the non-spherical distribution of the 3*d* valence electrons belonging to the ferrous or ferric ions and the non-spherical charge distribution of the neighboring ions in the crystalline lattice (Ingalls 1964). The valence contribution to the quadruple splitting is determined by a number of factors including the valence state and spin state. Of particular importance is the effect of crystal field on quadrupole splitting, which is mainly to lift the fivefold degeneracy of the 3*d* orbital states of the free iron atom or ion, splitting it into a series of orbital states of different wave functions and energies, which may collectively produce a non-spherical charge distribution at the position of the nucleus (Ingalls 1964).

Fig. 2 **a** Fractions of the three modeled iron sites as obtained from fits of the time spectra. The two Fe^{2+}-like sites have the same isomer shift but distinct quadrupole splittings. We labeled the Fe^{2+}-like site with the smaller quadrupole splittings as $Fe^{2+}{}_1$. This site was present at ambient pressure. The Fe^{2+}-like site with the larger quadrupole splittings appeared upon compression and was denoted as $Fe^{2+}{}_2$. Uncertainties are smaller than the symbols size. **b** Quadruple splitting values derived from the time spectra. The *size of the bars* gives the FWHM of the Gaussian broadening. Symbols at 12 GPa are horizontally offset by 1 GPa for visibility. Shown as references are the ranges of quadruple splitting values determined by conventional Mössbauer spectroscopy: 2H—high-spin Fe^{2+} in oxides at ambient conditions (Bancroft et al. 1967), 3H—high-spin Fe^{3+} in oxides at ambient conditions (Bancroft et al. 1967), $2L^6$—six-coordinate low-spin Fe^{2+} in FeS at 7.7 GPa and in pyrite FeS_2 and marcasite FeS_2 at ambient conditions (King et al. 1978), $3L^6$—one value for six-coorindate low-sin Fe^{3+} in Fe_2O_3 at 82 GPa and 4 K (Pasternak et al. 1999). **c** Isomer shift between the Fe^{3+}-like site and Fe^{2+}-like sites from fits of the time spectra. Shown as references are the ranges of isomer shift values determined by conventional Mössbauer spectroscopy: 3H2H—between high-spin Fe^{3+} (3H) and high-spin Fe^{2+} (2H) in oxides at ambient conditions (Bancroft et al. 1967), 3H2L—between high-spin Fe^{3+} (3H) in oxides and low-spin Fe^{2+} (2L) in pyrite FeS_2 and marcasite FeS_2 at ambient conditions (King et al. 1978). The lower end of the 3H2H range and the upper end of the 3H2L range extend beyond the scale of the plot

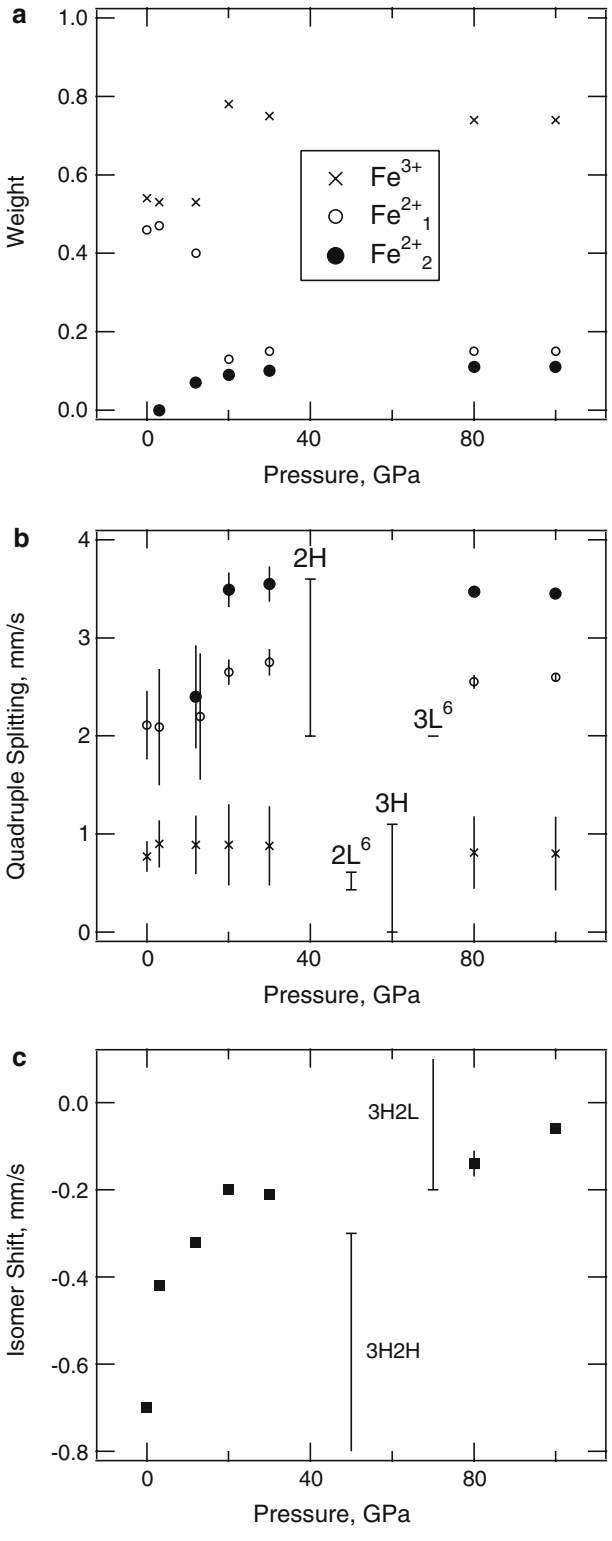

The 3*d* orbitals are grouped into two sets, a set of three known as the t_{2g} orbitals in which the charge density is localized between the coordinate axes, and a set of two known as the e_g orbitals in which the charge is localized along the coordinate axes. Compared with other configurations, a full ($3t_{2g}\uparrow 3t_{2g}\downarrow$ or $2e_g\uparrow 2e_g\downarrow$, where the up and down arrows denote spin-up and spin-down, respectively), half-full ($3t_{2g}\uparrow$ or $2e_g\uparrow$), or empty set corresponds to a more symmetric valence charge distribution, hence having a smaller contribution to the quadrupole splitting.

In the high-spin state, the quadrupole splitting of Fe^{2+} (2.0–3.6 mm/s for six- or eight-coordinate sites in oxides) is significantly larger than that of Fe^{3+} (0–1.1 mm/s for six-coordinate sites in oxides) (Bancroft et al. 1967). The large quadrupole splitting of high-spin Fe^{2+} may arise from the preferential population of the lowest level of the 3*d* orbitals ($3t_{2g}\uparrow 2e_g\uparrow 1t_{2g}\downarrow$, which is the case even for a cubic site, due to Jahn-Teller distortion), leading to an asymmetric valence charge distribution (Wertheim 1964). The small quadrupole splitting of high-spin Fe^{3+} can be attributed to the nearly spherical valence charge distribution in a half-full 3*d* subshell of Fe^{3+} ($3t_{2g}\uparrow 2e_g\uparrow$), especially when the crystal field is weak (Wertheim 1964).

Six-coordinate low-spin Fe^{2+} in sulfides exhibits relatively small quadrupole splitting values (0.4–0.6 mm/s) (King et al. 1978; Rueff et al. 1999), which may be explained by fully populated t_{2g} orbitals ($3t_{2g}\uparrow 3t_{2g}\downarrow$), corresponding to a highly symmetric valence charge distribution. One quadrupole splitting value was found for six-coordinate low-spin Fe^{3+} in Fe_2O_3 (2.0 mm/s at 82 GPa and 4 K, < 2.0 mm/s at 82 GPa and 300 K, Pasternak et al. 1999). The large quadrupole splitting of six-coordinate low-spin Fe^{3+} is consistent with the asymmetric valence charge distribution in the 3*d* subshell, where five electrons occupy three t_{2g} orbital ($3t_{2g}\uparrow 2t_{2g}\downarrow$). In several chemical compounds, the quadrupole splitting of six-coordinate iron at the intermediate-spin state is found indistinguishable from that of the low-spin state (Bancroft 1973), as expected from the equally asymmetric valence charge distribution.

Some relevant quadrupole splitting values for high-spin iron and six-coordinate low-spin iron are plotted in Fig. 2b to facilitate data analysis.

Literature on the quadrupole splitting of intermediate-spin and low-spin iron in 8–12-coordinate site is scarce. We try to make qualitative predications by considering the symmetry of valence charge distribution according to crystal field theory. In the 8–12-coordinate site, the e_g orbitals are at lower energy levels than the t_{2g} orbitals. The electronic configurations for the high-spin, intermediate-spin, and low-spin Fe^{2+} are $2e_g\uparrow 3t_{2g}\uparrow 1e_g\downarrow$, $2e_g\uparrow 2t_{2g}\uparrow 2e_g\downarrow$, and $2e_g\uparrow 1t_{2g}\uparrow 2e_g\downarrow 1t_{2g}\downarrow$, respectively, all having comparable symmetry. Consequently, a spin crossover in Fe^{2+} may not have any detectable effect on the quadrupole splitting. The electronic configurations of the intermediate-spin

or low-spin Fe^{3+} in the 8–12 coordinate site are $2e_g\uparrow 2t_{2g}\uparrow 1e_g\downarrow$, and $2e_g\uparrow 1t_{2g}\uparrow 2e_g\downarrow$, respectively, which are less symmetric than that of the high-spin state ($2e_g\uparrow 3t_{2g}\uparrow$), where all five orbitals are half-full. Therefore, the quadrupole splitting of 8–12-coordinate Fe^{3+} may increase upon a crossover to a lower spin state. These qualitative predications need to be tested by direct measurements and theoretical calculations.

In addition to the valence state, spin state, and coordination number, the quadrupole splitting is influenced by site distortion, which reduces the effects of valence charge distribution on quadruple splitting (Bancroft et al. 1967; Ingalls 1964). In several Al-free perovskite samples, the presence of multiple Fe^{2+}-like sites with distinct quadrupole splittings has been interpreted as a possible manifestation of the varying degrees of site distortion that arise from different next-neighbor configurations (Fei et al. 1994; McCammon et al. 1992). On the other hand, it has been shown that the quadrupole splitting of Fe^{3+} may be insensitive to lattice distortion (Burns and Solberg 1990).

Site occupancy of iron and lattice distortion

The valence state and spin state of iron in perovskite are intimately connected to the crystallographic site it occupies. Knowledge on the site occupancy of iron can greatly facilitate the interpretation of Mössbauer and X-ray emission spectra. Conversely, the hyperfine parameters extracted from Mössbauer spectra and the spin state information given by X-ray emission spectra may provide constraints on the site occupancy of iron. In perovskite, iron may take the 8–12-coordinate site (also known as the pseudo-dodecahedral site or the A site) and/or the six-coordinate site (also known as the octahedral site or the B site). Previous X-ray diffraction and spectroscopy measurements have concluded that Fe^{2+} resides in the A site (Fei et al. 1994; Jephcoat et al. 1999; McCammon et al. 1992; Shen et al. 1994). The site occupancy of Fe^{3+} is less clear and may depend on the Fe^{3+} content and/or Al content (Fei et al. 1994; Frost and Langenhorst 2002; Jephcoat et al. 1999; McCammon 1998). Atomistic simulation and element partitioning studies suggest that Fe^{3+} is likely to enter the A site through the coupled substitution: $^{A}Fe^{3+} + {}^{B}Al^{3+}(-){}^{A}Mg^{2+} + {}^{B}Si^{4+}$, especially with a relatively high Al content (Frost and Langenhorst 2002; Richmond and Brodholt 1998). Our sample contains comparable amounts of Fe^{3+} and Al^{3+}. Since the smaller trivalent cation Al^{3+} is expected to preferentially occupy the smaller B site, it is likely that the larger trivalent cation Fe^{3+} enters the A site. In a Mössbauer spectrum, the width of quadrupole splitting (expressed as FWHM in Table 1 and as the uncertainty on quadrupole splitting in Fig. 2) may be affected by the site occupancy of iron (Fei et al. 1994). At ambient conditions, the width of the quadruple splitting (0.31 ± 0.01 mm/s) is smaller than that of an Al-free PV sample (0.51 ± 0.10 mm/s, Jackson et al. 2005), suggesting single site occupancy by Fe^{3+}. On the basis of these considerations, it is very likely that both Fe^{2+} and Fe^{3+} are in the A site, although we cannot rule out that some iron might be in the B site.

The chemical formula of our sample $(Mg_{0.88}Fe_{0.09})(Si_{0.94}Al_{0.10})$ showed an apparent excess occupancy in the B site. This formula was derived from electron probe analyses alone, with the simplifying assumptions that all the iron is in the ferrous state and takes the A site, and that all the Al^{3+} takes the B site. Incorporating the constraints on the valence state of iron from Mössbauer spectroscopy measurements, and assuming that both Fe^{2+} and Fe^{3+} are in the A site, this formula becomes $(Mg_{0.87}Fe^{2+}_{0.04}Fe^{3+}_{0.05})(Si_{0.93}Al_{0.10})O_3$. There is still an apparent excess occupancy in the B site, indicating that at least a fraction of Al^{3+} resides in the A site.

There are two Fe^{2+}-like sites in our Al-PV sample under high pressure. Site reordering and variable site distortion are among possible origins for the development of the two sites with distinct quadrupole splittings. Our experiments were conducted at room temperature, under which condition site reordering does not seem possible. In Al-PV, different neighboring cation configurations may cause varying degrees of distortion (Li et al. 2005). If compression enhances the initial difference in the degree of distortion, then it may lead to the development of two sites. Another possible cause of variable site distortion is non-hydrostatic stress, which could cause deformation of the Fe–O polyhedra that varies with its orientation with respect to the directions of the principal stresses. If site distortion is the origin of the two Fe^{2+}-like sites, the appearance of the second Fe^{2+}-like site with a larger quadrupole splitting (Fig. 2) would indicate that a fraction of the Fe^{2+}-site become less distorted upon compression, reducing the lattice contribution to the quadrupole splitting (Ingalls 1964; McCammon 1998). Above 20 GPa, the values and widths of the quadrupole splitting of all three iron sites remain essentially constant, indicating strong resistance against further distortion of the local iron environment after initial compression.

Valence state and spin state of iron at ambient conditions

Basic properties of the lower mantle, including major element distribution and electrical conductivity,

depend critically on the valence state of iron in the predominant phase perovskite (e.g., Wood and Rubie 1996; Xu et al. 1998). Another potentially important parameter for geophysical models of the lower mantle is the spin state of iron in the host mantle phases, as it can influence the density, thermal conductivity, and element partitioning of the host phases (Burns 1993; Badro et al. 2003, 2004; Fei et al. 2005; Lin et al. 2005; Speziale et al. 2005; Sherman 1988). In Mössbauer spectroscopy, the valence state and spin state of iron may be determined based on the characteristic hyperfine parameters of iron. At ambient conditions, the large quadrupole splitting of the Fe^{2+}-like site and the large negative isomer shift between the Fe^{3+}-like site and Fe^{2+}-like sites indicate that the Fe^{2+}-like site is high-spin Fe^{2+}. The small quadrupole splitting of the Fe^{3+}-like site could be matched by high-spin Fe^{3+} or six-coordinate intermediate-spin or low-spin Fe^{2+}, which have similar hyperfine parameters and cannot be readily distinguished based on the Mössbauer data alone. Additional insight into the nature of the Fe^{3+}-site can be derived from the X-ray emission data. In XES, the intensity ratio between the Kβ' satellite peak and the K$\beta_{1,3}$ main peak reflects the number of unpaired electrons in the 3*d* sub-shell, which is determined by the valence state and spin state of iron (Fig. 3). Possible spin configurations can be deduced from a comparison between the calculated intensity ratios and observed values. If the 53% Fe^{3+}-like site at ambient condition is actually intermediate-spin or low-spin Fe^{2+}, then they will remain at the intermediate-spin or low-spin state during compression, because pressure can only induce a crossover toward a lower spin state. At 20 GPa, the observed intensity ratio is much higher than the expected value corresponding to 47% high-spin Fe^{2+} and 53% six-coordinate intermediate-spin or low-spin Fe^{2+}. Although the presence of a small fraction of six-coordinate intermediate-spin or low-spin Fe^{2+} cannot be excluded, the simplest interpretation that is consistent with both the Mössbauer and X-ray emission data at ambient condition is that the Fe^{2+}-like site is high-spin Fe^{2+}, and the Fe^{3+}-like site is high-spin Fe^{3+}. This conclusion supports the statement that no evidence has been found for the occurrence of low-spin iron in oxide at ambient conditions (Burns 1993).

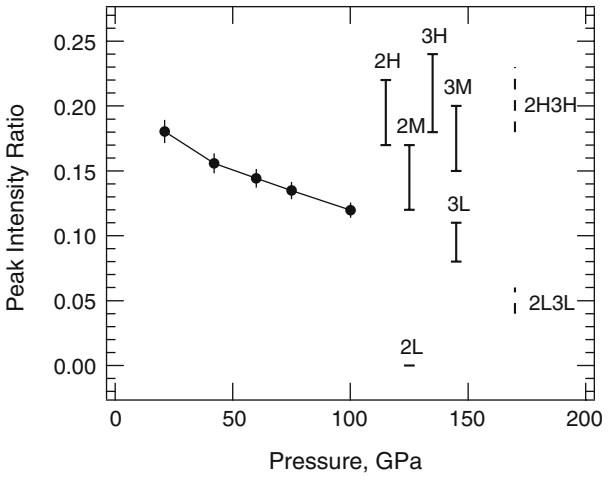

Fig. 3 Comparison between the observed and calculated intensity ratios between the Kβ' satellite peak at about 7.045 KeV (I') and the K$\beta_{1,3}$ main peak at about 7.058 KeV (I) in X-ray emission spectra of the Al-PV. *Solid circles with error bars* are experimental data (Li et al. 2004). *Vertical lines and a bar* shows the ranges or the value of intensity ratios calculated for various iron types, denoted by its valence state (2 = Fe^{2+}, 3 = Fe^{3+}) and spin state (*H* high-spin, *M* intermediate-spin, *L* low-spin). The intensity ratio for each iron type is calculated according to $I'/I = N/(N + 2)/c$, where N is the number of unpaired electrons in the incomplete 3*d* shell of iron, c is the empirical correction factor (Tsutsumi et al. 1976). The calculated ranges of intensity ratios reflect the range of values assigned to the correction factor c (between 3 and 4), arising from the uncertainty in the actual value of c for iron in the Al-PV and its possible variation with pressure, site occupancy, valence state, and spin state of iron. *Dashed lines* indicate the ranges of intensity ratios calculated for two possible spin states of iron in the Al-PV, by summing up contributions from all iron types according to $I'/I = \sum(f_i \cdot N_i/(N_i + 2))/c$, where the subscript i refers to a specific iron type, f_i refers to the fraction of i, N_i refers to the number of unpaired electrons in type i. The fraction of Fe^{3+} is 53% (Table 1) and does not change with pressure (the apparent change is attributed to a possible spin crossover)

Pressure effect on the valence state of iron

Pressure-induced valence state changes have been reported previously. Drickamer and coworkers observed reduction of ferric ion to ferrous ion under high pressure, probably due to charge transfer from ligand to metal (Champion et al. 1967). The reverse reaction, i.e. oxidation of ferrous ion to ferric ion, occurs in $Fe(OH)_2$ and was attributed to pressure-induced deformation of OH dipole (Pasternak et al. 2004). A third type of redox reaction, in which ferric ion decomposes to form ferric ion and iron metal at high pressure and high temperature, has been proposed to account for the ferric ion in perovskite samples synthesized from ferric-ion-free orthopyroxene starting materials (Fei et al. 1994; Frost et al. 2004; Lauterbach et al. 2000; Li et al. 2004; McCammon 1997). On the other hand, a recent synchrotron Mössbauer spectroscopy study found that pressure alone does not alter the valence state of iron in Al-free perovskite (Jackson et al. 2005).

In our Al-PV, the fraction of Fe^{3+}-like site, $Fe^{3+}/\sum Fe$, is about 50% at ambient conditions (Table 1;

Fig. 2). During the initial compression to 12 GPa, the fraction of the Fe^{3+}-like site barely changes. Between 12 and 20 GPa, it increases drastically to 75%, then remains essentially constant again up to the highest pressure of our experiments. The abrupt changes occur within a pressure range that is comparable to the observed structural and spin transition in iron metal (Rueff et al. 1999), suggesting that metallic iron may be present in the starting material or it may have been produced under high pressure through the above-mentioned self-redox reaction. However, the assumption of a minor amount of iron metal in the sample resulted in a significantly worse fit to the time spectra, and is therefore discarded. A simple charge balance calculation for iron gives an average charge of +2.5 at pressures below 12 GPa and +2.75 at pressures above 20 GPa. To account for the apparent increase in the average charge of iron by an oxidation reaction, half of the ferrous ion would have become ferric. At ambient conditions, the volume of the Al-PV sample is at least half of that of oxygen in the air that is trapped in the sample chamber (including that between the Al-PV grains). The density of the Al-PV is about four thousand times that of air. Although the iron content of the Al-PV is very low, the amount of O that is needed to oxidize half of the Fe^{2+} into Fe^{3+} is at least four times of the amount of free O in the sample chamber. Hence the increase in the fraction of the Fe^{3+}-like site between 12 and 20 GPa cannot be explained by an oxidation reaction. Given the lack of evidence for redox reaction and the insufficient supply of oxygen for oxidation reaction in the diamond cell, we consider it unlikely that the apparent valence change represents a real change in the valence state of iron. Between 20 and 100 GPa, the essentially constant fraction of ferric ion indicates that pressure alone does not alter the valence state of iron in the Al-PV within this pressure range.

Pressure-induced spin crossover

Although structurally stable to a depth that is greater than 2,000 km inside the Earth, pressure-induced changes in the electronic spin state of iron have been observed or indicated in both Al-PV and Al-free PV within the lower mantle pressure range (Badro et al. 2004; Jackson et al. 2005; Li et al. 2004). Unlike the well-known examples of spin transitions in pure Fe and FeS (Rueff et al. 1999), which are abrupt changes in the spin state accompanied by structural phase transitions, a number of studies indicate that the loss of magnetic moment in several perovskite samples occur gradually with increasing pressure (Jackson et al. 2005; Li et al. 2004, 2005). Iron in perovskite has multiple valence states and may occupy multiple crystallographic site, thus it may have a mixed spin state under certain pressure and temperature conditions (Li et al. 2004). X-ray emission data indicate the occurrence of intermediate-spin state in perovskite under high pressures (Li et al. 2004), although first-principle computations found the intermediate-spin state of Fe^{3+} unstable (Li et al. 2005). The possible occurrence of mixed spin state and intermediate-spin state introduces much complexity to the path of pressure-induced spin crossover in Al-PV. Additional challenges in resolving the path come from the uncertainties in the site occupancy of iron and the presence of pressure gradient and non-hydrostatic stress in the compressed sample. Amorphization of a perovskite sample under non-hydrostatic compression is another concern. A reduction of the non-hydrostatic stress on the sample may be achieved by annealing the sample using a laser beam. On the other hand, laser-annealing may lead to cation reordering or induce chemical reaction, thus affecting the electronic structure of iron in the sample. We did not anneal the compressed sample. The presence of several iron sites with distinct hyperfine parameters indicated that short-range order was preserved, even though long-range order might have been destroyed. Whether or not a significant degree of amorphization occurred under compression and how it affected the electronic structure of iron remains an issue of future investigation.

Independent constraints on the spin evolution of iron as a function of pressure may be derived from the synchrotron Mössbauer data. In fact, inferences on pressure-induced spin crossover in our sample between ambient conditions and 20 GPa are entirely based on the synchrotron Mössbauer data (Table 1; Fig. 2), as no X-ray emission measurements were performed within the pressure range that is outside the stability field of the Al-PV. Upon initial compression, the isomer shift between the Fe^{3+}-like site and the Fe^{2+}-like sites increases considerably, indicating that the *s*-electron density at the nucleus of the Fe^{2+}-like sites increase faster than that of the Fe^{3+}-like site, possibly because the Fe^{2+}-like sites are more compressible, and/or a gradual spin crossover takes place in the Fe^{2+}-like sites. Meanwhile, the widths of the quadrupole splittings increase significantly, with little changes in the values. If the isomer shift increase is due to a spin crossover in the Fe^{2+}-like sites, then the nearly constant quadrupole splitting value may imply that the Fe^{2+}-like sites belong to 8–12-coordinate Fe^{2+}, because the quadrupole splitting of six-coordinate Fe^{2+} decreases significantly upon a spin reduction, while that of 8–12-coordinate Fe^{2+} may be insensitive to the spin state. Between 12 and 20 GPa, the fraction of the

Fe^{3+}-like site increases abruptly, accompanied by reductions in the widths of the quadrupole splitting of the Fe^{2+}-like sites and an increase in the width of the quadrupole splitting of the Fe^{3+}-like site. The similarity between the hyperfine parameters of high-spin Fe^{3+} and six-coordinate intermediate-spin or low-spin Fe^{2+} suggest that a possible explanation for the apparent change in the valence state between 12 and 20 GPa is that six-coordinate Fe^{2+} undergoes a pressure-induced spin crossover from the high-spin to the intermediate-spin or low-spin state and appears as part of the Fe^{3+}-like site at 20 GPa (Fig. 2). The increase in the width of quadruple splitting of the Fe^{3+}-like site is consistent with the incorporation of intermediate-spin or low-spin Fe^{2+} with a slightly different quadrupole splitting value. It is likely that only the intermediate-spin state has been reached at 20 GPa, as the X-ray emission intensity ratio does not allow a significant fraction of low-spin iron to be present at this pressure, and the postulated spin crossover occurs within a pressure range that is considerably lower than that of the high-spin to low-spin crossover of Fe^{2+} in ferropericlase (60–70 GPa, Badro et al. 2003) and that of Fe^{3+} in hematite (50 GPa, Pasternak et al. 1999; Badro et al. 2002). This interpretation implies that six-coordinate Fe^{2+} is in the high-spin state at ambient conditions, which has been considered energetically unfavorable because of the mismatch in charge and ionic radius. On the other hand, if all the Fe^{2+} resides in the 8–12-coordinate site, a spin crossover may not have any detectable effects on its quadruple splitting, leaving the apparent change of valence state between 12 and 20 GPa unexplained. Since the hyperfine parameters of high-spin Fe^{2+} and intermediate-spin or low-spin Fe^{3+} may be comparable, one or both of the Fe^{2+}-like sites at 20 GPa could actually be intermediate-spin or low-spin Fe^{3+}. Accurate knowledge on the site occupancy of iron will be helpful in resolving the postulated spin crossovers outside the stability field of the Al-PV.

Between 20 and 100 GPa, the XES intensity ratio decreases continuously with increasing pressure, indicating the occurrence of one or more gradual spin crossovers towards lower spin states (Li et al. 2004). The reduction in the intensity ratio can be matched by a number of possible spin crossover paths which cannot be distinguished based on the XES data alone. General possibilities include (1) Fe^{2+} alone transforms to a lower spin state; (2) Fe^{3+} alone transforms to a lower spin state; and (3) both Fe^{2+} and Fe^{3+} transform to lower spin states. If spin reduction occurs in both Fe^{2+} and Fe^{3+}, the intensity ratio of the X-ray emission spectrum at 100 GPa indicates that both ions do not reach the final low-spin state at 100 GPa. An additional constraint on the spin evolution of iron is found in the synchrotron Mössbauer data (Fig. 2). Between 20 and 100 GPa, the isomer shift between the Fe^{3+}-like site and the Fe^{2+}-like sites increases slightly with increasing pressure, whereas the fractions of the three sites and associated values and widths of quadrupole splitting remain essentially constant. The increase in the isomer shift could be consistent with the possibilities (1) and (3) but is the opposite of what is expected for a spin reduction in Fe^{3+} alone. Thus, possibility (2) can be excluded. Based on the characteristic hyperfine parameters of iron that are described earlier, the nearly constant fractions and quadrupole splittings do not support a spin reduction on six-coordinate high-spin Fe^{2+} or high-spin Fe^{3+}. If the qualitative predictions based on crystal-field theory are applicable, and the symmetry of valence charge distribution is the dominant component in the quadrupole splitting of 8–12-coordinate iron, then the nearly constant quadrupole splittings would only allow an intermediate-spin to low-spin crossover between 20 and 100 GPa. Further understanding of the spin evolution requires quantitative modeling of the hyperfine parameters as a function of valence state, spin state, crystallographic site, and pressure, especially for the 8–12-coordinate site and the intermediate-spin state.

Conclusions

We show that the combination of synchrotron Mössbauer spectroscopy and XES can provide new constraints for the electronic structure of iron in Al-PV at ambient conditions and the spin evolution of iron under high pressures. Considering the broadening effect of temperature on spin crossover in lower mantle minerals (Sturhahn et al. 2005; Tsuchiya et al. 2006), such combination would be particularly useful for investigating the valence state and spin state of iron at simultaneous high pressure and high temperature that are prevalent in the Earth's interior. Additional complexities in the electronic structure of iron in Al-PV, such as the appearance of the second Fe^{2+}-like site and the apparent change in the fraction of Fe^{3+}-like site, are revealed by our Mössbauer study, which highlight the need for quantitative modeling of the hyperfine parameters of iron as a function of valence state, spin state, crystallographic site, and pressure, and the need for more accurate knowledge of the site occupancy of iron. The measured hyperfine parameters can be used to test and refine theoretical modeling of the electronic structure of iron in lower mantle perovskite.

Acknowledgements We thank Ross Angel at Virginia Tech for insightful discussions on the site occupancy of iron in perovskites, and for trying to perform a single-crystal X-ray diffraction measurement on our Al-PV sample. We thank Holger Hellwig at U. Illinois for helpful comments and suggestions on the early drafts of the manuscript. We thank Jinfu Shu at the Geophysical Laboratory for helping with the gasket preparation. We thank Catherine MaCammon at the Bayerisches Geoinstitut for helpful discussions on the effect of spin crossover on the Mössbauer characteristics of iron. We thank Dane Morgan at the University of Wisconsin–Madison for fruitful discussions on data interpretation. The manuscript benefited significantly from an anonymous review. This work is supported by National Science Foundation grant EAR-0337612. This work at LLNL was performed under the auspices of the US DOE at the UC/LLNL under contract no. W-7405-Eng-48. Support for the study was also provided by the Lawrence Livermore Fellowship to J. F. Lin.

References

Anderson DL, Bass J (1986) Transition region of the Earth's upper mantle. Nature 320:321–328

Badro J, Fiquet G, Struzhkin VV, Somayazulu M, Mao HK, Shen G, Bihan TL (2002) Nature of the high-pressure transition in Fe_2O_3 Hematite. Phys Rev Lett 89(20)

Badro J, Fiquet G, Guyot F, Rueff JP, Struzhkin VV, Vankó G, Monaco G (2003) Iron partitioning in Earth's mantle: toward a deep lower-mantle discontinuity. Science 300(5620):789–791

Badro J, Rueff JP, Vankó G, Monaco G, Fiquet G, Guyot F (2004) Electronic transitions in perovskite: possible nonconvecting layers in the lower mantle. Science 305:383–386

Bancroft GM (1973) Mössbauer spectroscopy. Halsted Press, Wiley, New York, p 252

Bancroft GM, Maddock AG, Burns RG (1967) Applications of the Mössbauer effect to silicate mineralogy—I. Iron silicates of known crystal structure. Geochim Cosmochim Acta 31:2219–2246

Burns RG (1993) Mineralogical applications of crystal field theory. Cambridge University Press, Cambridge, p 551

Burns RG, Solberg TC (1990) ^{57}Fe-bearing oxide, silicate, and aluminosilicate minerals. In: Coyne LM, S MSW, Blake DF (eds) Spectroscopic characterization of minerals and their surfaces, vol 415. American Chemical Society, Washington DC, pp 262–283

Champion AR, Vaughan RW, Drickamer HG (1967) Effect of pressure on the Mössbauer resonance in ionic compounds of iron. J Chem Phys 47:2583–2590

Eng PJ, Newille M, Rivers ML, Sutton SR (1998) Dynamically figured Kirkpatrick Baez X-ray microfocusing optics. SPIE Proc 3449:145

Fei Y, Virgo D, Mysen BO, Wang Y, Mao HK (1994) Temperature-dependent electron delocalization in $(Mg,Fe)SiO_3$ perovskite. Am Mineral 79:826–837

Fei Y, Zhang L, Corgne A, Watson HC, Shen G, Prakapenka V (2005) Spin transition in (Mg,Fe)O at high pressure. Eos Trans. AGU 86(52) Fall Meet Suppl, abstract

Frost DJ, Langenhorst F (2002) The effect of Al_2O_3 on Fe–Mg partitioning between magnesiowüstite and magnesium silicate perovskite. Earth Planet Sci Lett 199(1–2):227–241

Frost DJ, Liebske C, Langenhorst F, McCammon CA, Tronnes RG, Rubie DC (2004) Experimental evidence for the existence of iron-rich metal in the Earth's lower mantle. Nature 428:409–412

Ingalls R (1964) Electric-field gradient tensor in ferrous compounds. Phys Rev 133:A787–A795

Jackson JM, Sturhahn W, Shen G, Zhao J, Hu MY, Errandonea D, Bass JD, Fei Y (2005) A synchrotron Mössbauer spectroscopy study of $(Mg,Fe)SiO_3$ perovskite up to 120 GPa. Am Mineral 90:199–205

Jephcoat AP, Hriljac JA, McCammon CA, O'Neill HSC, Rubie DC, Finger LW (1999) High-resolution synchrotron X-ray powder diffraction and Rietveld structure refinement of two $(Mg_{0.95},Fe_{0.05})SiO_3$ perovskite samples synthesized under different oxygen fugacity conditions. Am Mineral 84:214–220

King H, Virgo D, Mao HK (1978) High-pressure phase transitions in FeS, using ^{57}Fe Mössbauer spectroscopy. Carnegie Inst Yearbook 77:830–834

Lauterbach S, McCammon CA, van Aken PA, Langenhorst F, Seifert F (2000) Mössbauer and ELNES spectroscopy of $(Mg,Fe)(Si,Al)O_3$ perovskite: a highly oxidised component of the lower mantle. Contrib Mineral Petrol 138:17–26

Li J, Struzhkin VV, Mao HK, Shu J, Hemley RJ, Fei Y, Mysen B, Dera P, Prakapenka V, Shen G (2004) Electronic spin state of iron in lower mantle perovskite. Proc Natl Acad Sci 101(39):14027–14030

Li L, Brodholt JP, Stackhouse S, Weidner DJ, Alfredsson M, Price GD (2005) Electronic spin state of ferric iron in Al-bearing perovskite in the lower mantle. Geophys Res Lett 32(L17307). DOI:10.1029/2005/GL023045

Lin JF, Shu J, Mao HK, Hemley RJ (2003) Amorphous boron gasket in diamond anvil cell research. Rev Sci Instrum 74(11):4732–4736

Lin JF, Struzhkin VV, Jacobsen SD, Hu MY, Chow P, Kung J, Liu H, Mao HK, Hemley RJ (2005) Spin transition of iron in magnesiowüstite in the Earth's lower mantle. Nature 436:377–380

Liu LG (1974) Silicate perovskite from phase transformations of pyrope–garnet at high-pressure and high-temperature. Geophys Res Lett 1:277–280

Mao HK, Xu J, Bell PM (1986) Calibration of the ruby pressure gauge to 800 kbar under quasihydrostatic conditions. J Geophys Res 91(B5):4673–4676

Mao HK, Xu J, Struzhkin VV, Shu J, Hemley RJ, Sturhahn W, Hu MY, Alp EE, Vočadlo L, Alfé D, Price GD, Gillan MJ, Schwoerer-Bohning M, Hausermann D, Eng P, Shen G, Giefers H, Lübbers R, Wortmann G (2001) Phonon density of states of iron up to 153 gigapascals. Science 292(5518):914–916

McCammon C (1997) Perovskite as a possible sink for ferric iron in the lower mantle. Nature 387:694–696

McCammon CA (1998) The crystal chemistry of ferric iron in $Fe_{0.05}Mg_{0.95}SiO_3$ perovskite as determined by Mössbauer spectroscopy in the temperature range 80–293 K. Phys Chem Miner 25:292–300

McCammon CA, Rubie DC, Ross II CR, Seifert F, O'Neill HSC (1992) Mössbauer spectra of $^{57}Fe_{0.05}Mg_{0.95}SiO_3$ perovskite at 80 and 198 K. Am Mineral 77:894–897

McCammon CA, Lauterbach S, Seifert F, Langenhorst F, van Aken PA (2004) Iron oxidation state in lower mantle mineral assemblages I: empirical relations derived from high-pressure experiments. Earth Planet Sci Lett 222:435–449

Pasternak MP, Rozenberg GK, Machavariani GY, Naaman O, Taylor RD, Jeanloz R (1999) Breakdown of the Mott-Hubbard state in Fe_2O_3: a first-order insulator–metal transition with collapse of magnetism at 50 GPa. Phys Rev Lett 82(23):4663–4666

Pasternak MP, Milner AP, Rozenberg GK, Taylor RD, Jeanloz R (2004) Pressure induced self-oxidation of $Fe(OH)_2$. Phys Rev Lett 92(8):085506

Richmond NC, Brodholt JP (1998) Calculated role of aluminum in the incorporation of ferric iron into magnesium silicate perovskite. Am Mineral 83(9–10):947–951

Rueff JP, Krisch M, Cai YQ, Kaprolat A, Hanfland M, Lorenzen M, Masciovecchio C, Verbeni R, Sette F (1999) Magnetic and structural alpha–epsilon phase transition in Fe monitored by X-ray emission spectroscopy. Phys Rev B 60:14510–14512

Shannon RD, Prewitt CT (1969) Effective ionic radii in oxides and fluorides. Acta Crystallogr Sect B25:925–946

Shen G, Fei Y, Hålenius UYW (1994) Optical absorption spectra of $(Mg,Fe)SiO_3$ perovskites. Phys Chem Miner 20:478–482

Sherman DM (1988) High-spin to low-spin transition of iron(II) oxides at high pressures: possible effects on the physics and chemistry of the lower mantle. In: Ghose S, Coey JMD, Salje E (eds) Structural and magnetic phase transitions in minerals, vol 7. Springer, Berlin Heidelberg New York, pp 113–128

Speziale S, Milner A, Lee VE, Clark SM, Pasternak M, Jeanloz R (2005) Iron spin transition in Earth's mantle. Proc Natl Acad Sci 102(50):17918–17922

Sturhahn W (2000) CONUSS and PHOENIX: evaluation of nuclear resonant scattering data. Hyperfine Int 125:149–172

Sturhahn W, Gerdau E (1994) Evaluation of time-differential measurements of nuclear-resonance scattering of X-rays. Phys Rev B 49(14):9285

Sturhahn W, Jackson JM, Lin JF (2005) The spin state of iron in minerals of Earth's lower mantle. Geophys Res Lett 32(L12307). DOI:10.1029/2005GL022802

Toellner TS (2000) Monochromatization of synchrotron radiation for nuclear resonant scattering experiments. Hyperfine Int 113:47–58

Tsuchiya T, Wentzcovitch RM, da Silva CRS, de Gironcoli S (2006) Spin transition in magnesiowüstite in Earth's lower mantle. Phys Rev Lett 96(19):198501

Tsutsumi K, Nakamori H, Ichikawa K (1976) X-ray Mn Kβ emission spectra of manganese oxides and manganates. Phys Rev B 13(2):929–933

Wertheim GK (1964) Mössbauer effect: principles and applications. Academic, New York

Wood BJ, Rubie DC (1996) The effect of alumina on phase transformations at the 660-kilometer discontinuity from Fe–Mg partitioning experiments. Science 273:1522–1524

Xu J, McCammon C, Poe BT (1998) The effect of alumina on the electrical conductivity of silicate perovskite. Science 282:922–924

Zha CS, Mao HK, Hemley RJ (2000) Elasticity of MgO and a primary pressure scale to 55 GPa. Proc Natl Acad Sci USA 97(25):13494–13499